Early post-ischemic glucose metabolism is dependent on function of TLR2: a study using [18F]FDG PET-CT in a mouse model of cardiac arrest and cardiopulmonary resuscitation

Rika Bajorat (rika.bajorat@med.uni-rostock.de)
Rostock University Medical Center: Universitatsmedizin Rostock

Jens Kurth
Rostock University Medical Center: Universitatsmedizin Rostock

Jan Stenzel
Rostock University Medical Center: Universitatsmedizin Rostock

Brigitte Vollmar
Rostock University Medical Center: Universitatsmedizin Rostock

Bernd J. Krause
Rostock University Medical Center: Universitatsmedizin Rostock

Daniel A. Reuter
Rostock University Medical Center: Universitatsmedizin Rostock

Tobias Schuerholz
Rostock University Medical Center: Universitatsmedizin Rostock

Stefan Bergt
Rostock University Medical Center: Universitatsmedizin Rostock

Research Article

Keywords: cardiac arrest, resuscitation, brain glucose metabolism, cerebral injury, [18F]FDG PET-CT, TLR2

Posted Date: April 13th, 2021

DOI: https://doi.org/10.21203/rs.3.rs-326507/v1

Early post-ischemic glucose metabolism is dependent on function of TLR2: a study using [^{18}F]FDG PET-CT in a mouse model of cardiac arrest and cardiopulmonary resuscitation

Rika Bajorat[1], Jens Kurth[3], Jan Stenzel[2], Brigitte Vollmar[4], Bernd J. Krause[3], Daniel A. Reuter[1], Tobias Schuerholz[1], Stefan Bergt[1]

Author information

Affiliations

[1]Department of Anesthesiology and Intensive Care Medicine, Rostock University Medical Centre, Rostock, Germany
[2]Core Facility „Multimodale Kleintierbildgebung“, Rostock University Medical Centre, Rostock, Germany
[3]Department of Nuclear Medicine, Rostock University Medical Centre, Rostock, Germany
[4]Institute of Experimental Surgery, Rostock University Medical Centre, Rostock, Germany

Corresponding author:

Dr. Rika Bajorat
Department of Anesthesiology and Intensive Care Medicine
Rostock University Medical Centre
Schillingallee 35
18057 Rostock, Germany
Tel.: +49 (0)381 494-6488
Fax: +49 (0)381 494-6483
Email: rika.bajorat@med.uni-rostock.de

Pages: 22

Figures: 6

Tables: 1

Words

Text: 5810 (including Abstract, Keywords, Declarations, Acknowledgments, List of abbrevations, References; excluding Title page with Affiliations, table and figures)
Abstract: 299

ABSTRACT

Purpose: An ischemic brain injury caused by cardiac arrest (CA) and cardiopulmonary resuscitation (CPR) affects cerebral function and presumably also brain glucose metabolism. The majority of patients who survive CA suffer from cognitive deficits and physical disabilities. Toll-like receptor 2 (TLR2) plays a cruical role in inflammatory response in ischemia and reperfusion (I/R). Since deficiency of TLR2 was associated with increased survival after CA-CPR, in this study glucose metabolism was measured using non-invasive [^{18}F]FDG PET-CT imaging before and early after CA-CPR in a mouse model comparing wild type (WT) and TLR2-deficient (TLR2$^{-/-}$) mice.

Methods: Two PET-CT scans using [^{18}F]FDG tracer were carried out to measure dynamic glucose metabolism before and early after CPR. To achieve this, anesthetized and ventilated adult female WT and TLR2$^{-/-}$ mice were scanned in PET-CT. After recovery from the baseline scan, the same animals underwent 10-minute CA followed by CPR and approximately 90 min after CA measurements of [^{18}F]FDG uptake were started. The [^{18}F]FDG standardized uptake values (SUVs) were calculated using PMOD-Software on fused FDG-PET-CT images with the included 3D Mirrione-Mouse-Brain-Atlas.

Results: The absolute SUV of glucose in the whole brain of WT mice was increased after CA-CPR. In contrast, the absolute glucose SUV in the whole brain of TLR2$^{-/-}$ mice was not significantly different between basal and measurements after CA-CPR. In comparison, basal measurements of both mouse strains show a significant difference in the whole brain absolute glucose SUVs, whereby TLR2$^{-/-}$ mice revealed 34.6% higher values. The altered mouse strains presented a different pattern in glucose uptake under normal and ischemic conditions.

Conclusion: There is evidence that the post-ischemic differences in glucose metabolism were associated with the function of TLR2 and that PET-CT imaging could be useful as an additional methodology in assessing diagnosis and prognosis during post-cardiac arrest care. Further studies are needed.

Keywords: cardiac arrest, resuscitation, brain glucose metabolism, cerebral injury, [^{18}F]FDG PET-CT, TLR2

DECLARATIONS

Funding

This work was supported by the FORUN Research Program of the Rostock University Medical Center.

Conflict of interest/Competing interests

None of the authors has any conflict of interest to disclose. We confirm that we have read the Journal's position on issues involved in ethical publication and affirm that this report is consistent with those guidelines.

Availability of data and material

The datasets used and/or analyzed during the current study are available from the corresponding author on reasonable request.

Code availability

Software application or custom code are available from the corresponding author on reasonable request.

Authors´contributions

Conceptualization: Stefan Bergt, Rika Bajorat, Bernd J. Krause; *Methodology:* Stefan Bergt, Rika Bajorat, Jan Stenzel; Formal analysis and investigation: Rika Bajorat, Jens Kurth, Jan Stenzel; *Writing - original draft preparation*: Rika Bajorat; *Writing - review and editing:* Rika Bajorat, Jens Kurth, Brigitte Vollmar, Bernd J. Krause, Daniel A. Reuter, Tobias Schuerholz, Stefan Bergt; *Funding acquisition*: Stefan Bergt, Rika Bajorat; *Resources:* Brigitte Vollmar, Bernd J. Krause, Daniel A. Reuter, Tobias Schuerholz; *Supervision:* Brigitte Vollmar, Bernd J. Krause, Daniel A. Reuter

Ethics approval

All procedures were performed according to national and international guidelines on the ethical use of animals (European Communities Council Directive 86/609/EEC). The experimental protocol was approved by the Ethical Committee for Care and Use of Laboratory Animals (local authority: Landesamt für Landwirtschaft, Lebensmittelsicherheit und Fischerei (LALLF) Mecklenburg-Vorpommern, permission number: LALLF M-V/TDS/7221.3-1-068/15). All efforts were made to minimize animal suffering and to reduce the number of animals used.

Consent to participate

Not applicable

Consent to publication

Not applicable

INTRODUCTION

Out-of-hospital cardiac arrest (OHCA) strikes every year about 95.9/100,000 adults worldwide (1). Prognosis remains very poor: European data shows an in-hospital mortality of nearly 90% of patients (2, 3). And even in survivors in particular neurological prognosis is very limited. In consequence, only less than 10% of patients return to a self-controlled live (4, 5). The major mechanism for cerebral damage is of course the circulatory arrest that directly leads to a lack of oxygenation of brain tissue (6). Persistent hypoxemia further aggravates global cerebral ischemia and the induced neuronal cell damage (7). Although cardiopulmonary resuscitation (CPR) and return of spontaneous circulation (ROSC) lead to cerebral reperfusion and oxygenation, a further consequence is a severe ischemia-reperfusion (I/R) injury leading to an excessive systemic inflammatory response, often called post-cardiac arrest syndrome (8, 9). Cerebral inflammation is characterized by activation of glial cells, influx of peripheral immune and inflammatory cells, high concentrations of reactive oxygen species (ROS) and release of pro-inflammatory mediators such as cytokines and adhesion molecules (10-12). Toll-like receptors are an integral part of the innate immune response in many pathologies. In particular TLR2 plays a central role in activation of inflammatory response under I/R. It initiates downstream signal pathways to induce the release of pro-inflammatory cytokines such as TNF-α, iNOS, IL-1β and ICAM-1 (13, 14). Further, TLR2 mediates crosstalk between the cellular and humoral innate immune response (15). So TLR2 is also involved in the immunological response to ischemic brain injury (16-19). Interestingly, TLR2-deficient ($TLR2^{-/-}$) individuals displayed less discharge of pro-inflammatory cytokines improved survival after CA-CPR in the mouse model (20).

The human brain consumes about one fifth of the whole body's glucose as its primary source of energy with very complex regulatory mechanisms (21, 22). Monitoring cerebral glucose metabolism therefore might enable to add functional information on the extent of cerebral damage, its recovery, and potentially also assessment of neurological prognosis. Positron emission computed tomography (PET-CT) with the use of [^{18}F]FDG (2-[^{18}F]fluoro-2-deoxy-D-glucose) as tracer allows to investigate cerebral glucose metabolism. There are stimulating study results using this method in in different models of neuronal diseases, and also in hypoxic-ischemic and traumatic brain injury (23-25). But so far there are only sparse data regarding cardiac arrest brain injury (26, 27).

Therefore we investigated brain glucose metabolism with [^{18}F]FDG PET-CT in wild type (WT) and TLR2-deficient mice before induction of CA (basal metabolism) and early after CA-CPR.

MATERIALS AND METHODS

Animals

Female wild type (WT, C57BL/6J, n=14) and TLR2-deficient (TLR2$^{-/-}$, B6.129-Tlr2^{tm1Kir}/J, n=13) 4-5-month-old mice were used with a body weight of approximately 20 g each. Animals were housed in a temperature-controlled environment (22°C) under a 12:12 h dark/light cycle with free access to water and food.

All procedures were performed according to national and international guidelines on the ethical use of animals (European Communities Council Directive 86/609/EEC). The experimental protocol was approved by the Ethical Committee for Care and Use of Laboratory Animals (local authority: Landesamt für Landwirtschaft, Lebensmittelsicherheit und Fischerei (LALLF) Mecklenburg-Vorpommern, permission number: LALLF M-V/TDS/7221.3-1-068/15). All efforts were made to minimize animal suffering and to reduce the number of animals used.

Study groups and Experimental protocol

Two groups of mice, WT- and TLR2$^{-/-}$ mice, were studied. Each group consisted of ten animals for analysis. The experimental protocol, which is outlined in detail in figure 1, envisaged baseline PET imaging, recovery from anesthesia for at least 7 days, followed by a standardized model of cardiac arrest and resuscitation, and then followed by a post-intervention PET imaging.

Anesthesia

All interventions (baseline PET imaging, cardiac arrest and resuscitation, post-intervention PET imaging) were performed under general anesthesia. Mice were anaesthetized by intraperitoneal injection of 12 µg/g ketamine and 8 µg/g xylazine and subjected to oral intubation and mechanical ventilation (0.4 fraction of inspired oxygen (FiO_2), tidal volume of 10 µl/g, respiratory rate of 120 breaths per minute).

Positron Emission Tomography Imaging

Baseline and post-intervention [^{18}F]FDG PET studies were performed in a small animal PET-CT (Siemens Inveon PET-CT, Siemens Healthineers, Erlangen). Animals together with the ventilator were carefully transferred to the PET bed and fixed. The acquisition of 60-min dynamic PET as list mode data set was started immediately before the injection of [^{18}F]FDG (2-[^{18}F]fluoro-2-deoxy-D-glucose) in 0.2 ml normal saline (table 1), which was injected via tail vein catheter at baseline and post-intervention via central venous catheter.

All PET studies were reconstructed as series 3D PET images of multiple frames with various time durations (15 x 20 sec; 10 x 60 sec; 9 x 300 sec) using a 2D-ordered subsets expectation maximization algorithm (four iterations, six subsets) resulting in a voxel size of 0.86 mm × 0.86 mm × 0.79 mm. Whole body CT scan was used for attenuation correction and PET studies were also corrected for random coincidences, dead time, scatter and decay.

Cardiac Arrest and Resuscitation

The model of CA-CPR was conducted as described previously (20, 28). Briefly, the anesthetized and mechanically ventilated mice were placed on an auto-regulated heating plate to prevent cooling. Body temperature was continuously monitored by rectal thermocouple probe (Effenberger, Pfaffingen, Germany). Needle probe electrocardiography (ECG; Animal bio Amp, ADInstruments, NSW, Australia) monitoring was initiated. Blood pressure was observed using a non-invasive blood pressure device (NIBP Controller, ADInstruments, NSW, Australia). Data acquisition occurred digitally (LabChart 5 pro, ADInstruments, NSW, Australia). A central venous catheter (CVC; PE50, ID 0.28 mm; Portex, Hythe, UK) was inserted into the right jugular vein. CA was induced by injection of 80 µg/g potassium chloride (KCl 7.45%; B. Braun Melsungen AG, Melsungen, Germany), and mechanical ventilation was interrupted upon verification of CA by electrocardiography. Resuscitation was initiated following 10 min of CA, precordial chest compressions were begun with a frequency of 450/min using a modified sewing machine, 0.4 µg/g epinephrine (Adrenalin 1:1000, InfectoPharm GmbH & Co. KG, Heppenheim, Germany) was injected and ventilation was resumed (220/min; FiO_2 1.0). After 2 min of CPR, respiratory rate was reduced to 120/min, FiO_2 to 0.6 and turned to FiO_2 0.4 after 20 min of successful resuscitation. After ROSC all animals were fluid resuscitated by intravenous application of 200 µl of

isotonic saline (B. Braun Melsungen AG, Melsungen, Germany). One hour after ROSC the post-intervention PET studies were performed as described above.

Image analysis

Image analysis was performed using PMOD v3.7 (PMOD Technologies LLC, Zurich, Switzerland). For standardized delineation of the target regions the implemented T2-weighted mouse brain MR template by Mirrione et al. was used (29, 30). The animal-specific CT datasets were spatially normalized to the MRI dataset of this atlas. The respective transformation matrices were used to also normalize the PET datasets into the Mirrione matrix. All transformations were performed using rigid matching algorithm as implemented in PMOD. The predefined region VOIs of the Mirrione atlas were used to extract time-activity curves (TAC) from the dynamic PET data. To also determine the static uptake in the defined brain regions, the last three frames of the dynamic data set (15 min) were averaged. The uptake values were presented as standardized uptake value (SUV) and were obtained by normalizing tissue radioactivity concentration to injected dose and body weight of the specific animal.

Statistics

Results are shown as median and mean ± standard error of the mean (SEM). Differences in glucose uptake were assessed and significance was tested using Wilcoxon rank-sum test for related and Mann-Whitney *U* test for independent samples (SPSS 22). With respect to significance, we first set the level of significance to $p \leq 0.05$. To account for multiple testing Bonferroni correction was used. On the basis of the known variance of individual experiments the effect sizes r were determined ($r = Z/\sqrt{n}$; $r < 0.1$: weak, $0.1 \leq r < 0.3$: mean, $r > 0.5$: large). To evaluate the kinetics of dynamic measurements the curves were parted according to curve progression in an exponential and a linear part. For evaluation of correlation a logarithmic or linear regression was used. Correlation coefficient R was calculated and therefore: $|R| <$ 0,1: slight correlation; $0,1 \leq |R| <$ 0,3: moderate correlation; $|R| >$ 0,5: strong correlation. Determination coefficient R^2 represents a measurement for the goodness-of-fit and was used for the regression lines in figure 3.

RESULTS

14 animals were studied in WT group, and 13 animals in the TLR2$^{-/-}$ group. Due to technical or medical complications or unsuccessful CPR, 4 animals in the WT group, and 3 animals in the TLR2$^{-/-}$ group had to be excluded. Accordingly, in each group 10 animals could be involved in data analysis. Hemodynamic, as well as procedural data of CPR and PET-scans are given in table 1 and did not differ between both groups.

Increased uptake of glucose in WT mice after cardiac arrest and cardiopulmonary resuscitation

Absolute uptake values determined in PET-CT images analysis (Fig.2) showed an increase of glucose uptake over time (Fig.3). Data showed an exponential increase at the first 400 s of all measurements. In this part the kinetics were almost the same, supported by a strong positive correlation R between basal and PET scans after CA-CPR (WT: R=0.986051; TLR2$^{-/-}$: R=0.996367). As well, no difference appeared in the kinetics of exponential glucose uptake in basal PET scans over time among the mouse strains seen by a strong positive correlation (WT vs. TLR2$^{-/-}$: R=0.968828). After the saturation of glucose uptake, the curve followed a linear course with a slight slope compared to the maxima (Fig.3). The correlation coefficients displayed strong positive correlation within the TLR2$^{-/-}$ animal group between basal and PET scans after CA-CPR (R=0.844897), and in comparison with the basal PET scans (WT vs. TLR2$^{-/-}$: R=0.961172). In the WT animals we found a moderate positive correlation in the curve progression (basal vs. after CA-CPR: R=0.161897). The analysis of correlation shows that glucose uptake followed very similar kinetics over time in investigated groups and basal and PET scans after CA-CPR.

When analyzing the last 15 minutes of measurement and plotted as absolute [^{18}F]FDG uptake, a difference in quantity of glucose uptake could be revealed (see Fig.4). The absolute uptake of [^{18}F]FDG in the whole brain was significantly higher in WT animals after CA-CPR in comparison with basal measurements (basal SUV_{mean}: 0.882 ± 0.055 vs. CA-CPR SUV_{mean}: 1.108 ± 0.021; n=10, p=0.017, r=0.757 (large effect size), Wilcoxon rank-sum test, Bonferroni corrected). There was about 25.6% more glucose uptake in the brain approximately 140 minutes after CA-CPR. In contrast, the absolute glucose uptake in the whole brain of TLR2$^{-/-}$ mice was not significantly different between basal and measurements after CA-CPR (basal SUV_{mean}: 1.187 ± 0.031 vs. CA-CPR SUV_{mean}: 1.120 ± 0.036; n=10, p=0.114, Wilcoxon rank-sum test), but the

trend showed that mean glucose uptake after CA-CPR was 6.02% lower than basal measurements. Hence, the different mouse strains presented a different pattern in glucose uptake under normal conditions, and after CPR.

Basal glucose uptake is much higher in TLR2$^{-/-}$ mice

In comparison, basal measurements of both mouse strains, WT vs. TLR2$^{-/-}$, show a highly significant difference with regards to the absolute glucose uptake in the whole brain (n=10, p=0.001, r=0.71 (large effect size), Mann-Whitney U test, Bonferroni corrected). Basal mean glucose uptake values of WT mice were SUV_{mean} 0.882 ± 0.055 and in TLR2$^{-/-}$ mice the glucose uptake displayed with SUV_{mean} 1.187 ± 0.031 was about 34.6% higher (Fig.4). Further, the differences in the brain regions in absolute [^{18}F]FDG uptake values between the animal strains in basal PET scans were investigated and are given in figure 5. The higher absolute SUV of glucose in TLR2$^{-/-}$ mice extended in basal measurements significant over all brain regions in comparison to the WT mice (Fig.5). The p values also were calculated using Mann-Whitney-U-test and Bonferroni correction and range between p=0.000 for olfactory bulb as well as cerebellum and p=0.011 for hypothalamus (Fig.5).

Pattern of glucose uptake in various brain regions differs between WT and TLR2-deficient mice after cardiac arrest and cardiopulmonary resuscitation

In the WT animals, the absolute glucose uptake was increased after CA-CPR (Fig.6a) in every brain region. Significant uptake increase was found the basal forebrain, superior colliculi, inferior colliculi, hypothalamus, amygdala, midbrain, cerebellum and brain stem using the Wilcoxon rank-sum test. The increase of the SUV in olfactory bulb, cortex and striatum was not significant with a difference under 17%. The increase ranged overall between 12.02% in the striatum and 42.04% in the hypothalamus (Fig.6b).

Unlike in the group of TLR2$^{-/-}$ mice, in general a decreased uptake of glucose after CA-CPR compared to the basal measurements was noted. Significant differences (Wilcoxon rank-sum test) were found in the olfactory bulb, cortex, striatum and hippocampus (Fig.6c). The decrease of glucose uptake ranked between -13.91% (striatum) to -1.22% (cerebellum). In contrast, in two brain regions, namely the hypothalamus (5.74%) and brain stem (0.23%), a statistically non-significant increase was observed (Fig.6d).

When looking at the results of absolute data of investigated animal groups, apart from

the fact that WT mice generally exhibited an increase and TLR2$^{-/-}$ a decrease of glucose uptake, the regions that were significantly different when comparing basal and measurements after CA-CPR were partly opposite (Fig.6a,c). Whereas in TLR2$^{-/-}$ mice significant differences in forebrain occurred (Fig.6: red text and insert), this was not the case in the same brain areas of WT animals. In the WT group, the significant differences were detected in the posterior cortical areas (= hindbrain; Fig.6: Insert).

DISCUSSION

The present study strengthens the evidence that cerebral glucose uptake increases in the early phase after CA and CPR, and that this effect can be assessed by [^{18}F]FDG PET. Our data is the first that quantifies that effect at the early phase after CPR in a murine model measuring the same animals before and after intervention. Further, this study primarily shows that this effect of enhanced glucose uptake is extenuated in TLR2-deficient individuals.

Enhanced absolute glucose uptake in the brain of WT mice early after CA-CPR

It is widely agreed that the acute phase of cerebral hypoxic injury produces a marked depression of cerebral glucose metabolism that persists for several hours in various species (31, 32, 26). Decreased glucose consumption could be explained by neuronal cell damage and following insufficiency or loss of transmitting impulses in neuronal cells (22). In contrast to descriptions of decreasing brain metabolism after CA-CPR, in WT mice we found enhanced absolute glucose uptake early after CA-CPR for all brain regions and this increase reached significance in the hindbrain. Investigations done with a comparable mouse model of CA-CPR also discovered significant increases in [^{18}F]FDG uptake in the brain of mice 72 hours post-CA (27). Zhang et al. (27) chose with 72 hours a considerably later time point for [^{18}F]FDG-PET imaging, which possibly reflects progression of late brain injury. They speculate whether mitochondrial respiration is suppressed by CA induced brain injury in the used animal model (27). The results could therefore reflect an increase in glucose uptake due to a switch of glucose metabolism from oxidative respiration to glycolysis, similar to the Warburg effect in cancer (27). It is obvious to assume that this switch of glucose metabolism occurred at an early time point after CA, but has yet to be proven. Although the etiology of increased glucose metabolism is unclear and some earlier studies show an impaired

glucose metabolism after cardiac arrest (32, 33, 26), an increased glucose metabolism can be also explained by the upregulated inflammatory response initiated with hypoxic impairment. For several immune cells including macrophages, T cells and neutrophils, in particular if they are activated, elevated glycolysis has been described. Activated and infiltrating inflammatory cells utilize glucose at a much higher level than peripheral non-inflammatory cells (34, 35, 23). An early increase in [^{18}F]FDG uptake in the whole brain with high significance in cortex and cerebellum was observed five hours following the induction of systemic inflammation like sepsis-associated encephalopathy in mice (25). The authors observed significantly enhanced [^{18}F]FDG uptake values in cortex and cerebellum, but in the hippocampus, the values failed to reach significance (25). Simultaneously they found a significantly higher number of activated microglia per area and percentage of total microglia in all investigated brain regions (25). Activated microglia and infiltrating peripheral immune cells in the brain seem to rely on very efficient glucose transporters which are able to extract high amounts of glucose even in ischemic tissue and therefore can contribute to [^{18}F]FDG PET signal during neuroinflammation (36). After stimulation of the immune system with TLR ligands, B cells increase their glucose consumption very early after treatment and these cells respond to TLR treatment with high uptake of [^{18}F]FDG in *in vitro* measurements (37). Such findings could explain the rise in [^{18}F]FDG uptake we measured and make them the most likely cause of the increase as CA-CPR induces cerebral inflammatory processes. Hosmann et al. (38) established a microdialysis setting *in vivo* to investigate the impact of resuscitation methods on cerebral and peripheral metabolism for lactate, glucose and glutamate simultaneously. Their results that cerebral glucose levels fell below the detection limit during CA-CPR, returned to baseline level after ROSC and are significantly elevated 16 to 48 min after ROSC, support our findings (38). As previously mentioned, Zhang et al. discovered a rise in glucose uptake 72 h post-CA with significance in the hindbrain, in contrast, the increase in the regions of the forebrain failed to reach significance (27) corresponding to our results presented for the immediate period after ROSC.

TLR2$^{-/-}$ mice showed no difference between basal brain glucose uptake and early after CA-CPR but displayed higher glucose level than WT mice

In WT mice an increase of [^{18}F]FDG uptake after CA-CPR was observed, whereas in TLR2$^{-/-}$ mice no difference of [^{18}F]FDG uptake between basal and post-CA-CPR measurements was detected. As described for rats, the cerebral glucose levels also

possibly fall during CA-CPR in TLR2$^{-/-}$ mice and return to normal after ROSC (38), but do not rise immediately after ROSC. Maybe at this early point in time when the PET scans were done, the lack of TLR2, one of the key innate immune sensors, restricted the signaling of early immune response that usually occur under I/R damage. The TLR2$^{-/-}$ mouse strain has shown a reduced increase in immune response eight hours following CA-CPR as well (20). Hence, the mouse strains used for the study presented completely different pattern of glucose uptake at basal and after CA-CPR. An earlier study done with the same mouse strains and the same animal model of CA-CPR described a different increase of plasma levels between WT and TLR2$^{-/-}$ mice eight hours following CA-CPR such as interleukin-6 (IL-6) in WT group was increased about 100-fold, whereas in TLR2$^{-/-}$ group the increase was only 5 times (20). These differences in the increase of inflammation markers in the mouse strains used support the assumption that elevated inflammation raises the need for glucose. In addition to a reduced increase of inflammation markers, Bergt at al. (20) revealed evidence that a lack or inhibition of TLR2 signaling is associated with improved survival and upgraded preservation of motor function and cognitive capacity following CA-CPR. Activation of TLR2 initiate the transcription of genes associated with innate immune responses and inflammation, that leads to tissue injury by initiation of apoptotic pathways also in the brain (17). So the lack of TLR2 could explain the equal levels of glucose uptake basal and after CA-CPR in the brain, because of the significant lower inflammatory reaction in TLR2$^{-/-}$ mice after CA-CPR (20). Information on the role of TLR2 deficiency in cerebral I/R injury are varying. In addition to inflammatory signals leading to tissue injury, TLR2 induces also protective signals that result in production of cytoprotective molecules such as heat shock proteins and Bcl-2, an anti-apoptotic molecule (39). There are suggestions that activation of innate immunity in the brain is an ambiguous event that can be advantageous or disadvantageous for the fate of the host depending on the specific conditions of neuronal injury and the balance between inflammatory and protective signals (40). Such a balance may affected by different expression levels which were changing dependent on age (41).

If we consider the results of basal glucose uptake and following CA-CPR, the different patterns of glucose uptake detected amongst the mouse strains support the important well-known role of TLR2 in inflammatory reaction and now extend to a potential cross-link to energy metabolism. These results could lead to additionally using glucose metabolism as a method for predicting the course of inflammation in post-cardiac arrest syndrome.

Higher basal glucose level in TLR2$^{-/-}$ mice

In our study the basal absolute brain glucose uptake values in the TLR2$^{-/-}$ mice were much higher than in WT mice. To address these differences in the basal glucose metabolism further investigations for characterizing the normative profile of WT and TLR2$^{-/-}$ mice have to be done. The effects of sex, age and cognition on normal cerebral glucose metabolism in humans were investigated, but results were inconsistent (42). No studies for rodents were found. There is a general consensus that reduction in brain metabolism with age tends to occur in the anterior part of the brain (43). Sex-specific effects can be excluded as only female mice were investigated in this study, but in general sex-specific aging effects on brain metabolism may also exist (42).

Study Limitations

However, our present study has some limitations. First, the use of anesthesia during the experimental procedure may have affected the distribution of brain glucose metabolism, as anesthesia, especially use of ketamine/xylazine, is known to reduce metabolism throughout the murine brain and result in a lower uptake of [^{18}F]FDG compared to isoflurane or awake (44). At the same time, ketamine/xylazine anesthesia generate increased blood glucose levels (44), due to a known pharmacological effect of xylazine. Here, xylazine is an alpha-2-adrenergic receptor agonist blocking insulin release to the blood leading to a hyperglycemic state (45). Because of the experimental setting in the present study, it has to be taken into consideration that all basal PET scans recordings were started after induction of anesthesia, tail vein catheter and bedding, whereas PET scans following CA-CPR were started about two hours after induction of anesthesia. At that time the effect of anesthesia was decreased and the mice were at rest and still unconscious. Second, after CPR only one time point was studied. We were interested in mechanisms of the early phase after global ischemic insult, because this is the phase for diagnostics and concentrated efforts to find the optimal treatment strategy. Third, furthermore FDG-PET provides information about the uptake of glucose and the first part of glycolysis but does not evaluate glucose metabolism beyond this (46). Fourth, the application of FDG-PET for imaging of neuroinflammation is basically also limited (47). That neurodegeneration also decreases glucose consumption, can be neglected for our study, because all used animals were at the same age, young adults.

CONCLUSION

We found that cardiac arrest and resuscitation induced a different glucose metabolism post-ischemia associated with the function of key immune factor TLR2 compared to the basal grade of glucose metabolism. Upcoming experiments will be focused on the different basal glucose uptake in TLR2-deficient mice. PET targeting brain metabolism and further development of new tracers provide new tools to track the progression of diseases. The biochemical characteristics of PET tracers may help uncover the pathophysiological changes in the brain after ischemic injury. [^{18}F]FDG PET-CT imaging can potentially add useful information for a more accurate diagnosis during post-cardiac arrest care, but more studies on PET-based predictions on the outcome are needed. Future studies should be focused on the complex biochemical and cellular regulation and functional brain pathophysiology considering the interplay of energy metabolism and cellular function.

List of abbreviations

CA	cardiac arrest
CPR	cardiopulmonary resuscitation
CA-CPR	cardiac arrest and cardiopulmonary resuscitation
TLR2	toll-like receptor 2
I/R	ischemia and reperfusion
PET-CT (PET)	positron emission computed tomography
[^{18}F]FDG	2-[^{18}F]fluoro-2-deoxy-D-glucose
CT	computed tomography
WT	wild type
TLR2$^{-/-}$	TLR2-deficient
SUV	standardized uptake value
FiO_2	fraction of inspired oxygen
ROSC	return of spontaneous circulation
ROS	reactive oxygen species
TAC	time-activity curves

Acknowledgements

We thank Romina Rauer and Anne Möller for excellent technical assistance and Ulrike Schlüter for suggestions for manuscript. This work was supported by the FORUN Research Program of the Rostock University Medical Center.

REFERENCES:

(1) Porzer M, Mrazkova E, Homza M, Janout V. Out-of-hospital cardiac arrest. Biomed Pap Med Fac Univ Palacky Olomouc Czech Repub. 2017;161:348-353. https://doi.org/10.5507/bp.2017.054

(2) Benjamin EJ, Virani SS, Callaway CW, et al. Heart Disease and Stroke Statistics-2018 Update: A Report From the American Heart Association. *Circulation*. 2018;137:e67-e492. https://doi.org/10.1161/ CIR.0000000000000558

(3) Gräsner JT, Lefering R, Koster RW, et al. EuReCa ONE-27 Nations, ONE Europe, ONE Registry: A prospective one month analysis of out-of-hospital cardiac arrest outcomes in 27 countries in Europe. *Resuscitation*. 2016;105:188-195. https://doi.org/10.1016/j.resuscitation.2016.06.004

(4) Mozaffarian D, Benjamin EJ, Go AS, et al. American Heart Association Statistics Committee and Stroke Statistics Subcommittee. (2015) Heart disease and stroke statistics--2015 update: a report from the American Heart Association. *Circulation*. 2015;131(4):e29-322. https://doi.org/10.1161/CIR.0000000000000152

(5) Püttgen HA, Pantle H, Geocadin RG. (2009) Management of cardiac arrest patients to maximize neurologic outcome. *Curr Opin Crit Care*. 2009;15:118-24. https://doi.org/10.1097/ MCC.0b013e328326077c

(6) Neumar RW, Nolan JP, Adrie C, et al. Post-cardiac arrest syndrome: epidemiology, pathophysiology, treatment, and prognostication. *Circulation.* 2008;118:2452-83. https://doi.org/10.1161/ CIRCULATIONAHA.108.190652

(7) Miyamoto O and Auer RN. Hypoxia, hyperoxia, ischemia, and brain necrosis. *Neurology*. 2000;54:362-362. DOI: 10.1212/wnl.54.2.362

(8) Geocadin RG, Koenig MA, Jia X, Stevens RD, Peberdy MA. Management of brain injury after resuscitation from cardiac arrest. Neurol Clin. 2008;26(2):487-506. https://doi.org/10.1016/j.ncl.2008.03.015

(9) Liu F and McCullough LD. Inflammatory responses in hypoxic ischemic encephalopathy. *Acta Pharmacol Sin*. 2013;34:1121-1130. https://doi.org/10.1038/aps.2013.89

(10) Lucas SM, Rothwell NJ, Gibson RM. The role of inflammation in CNS injury and disease. Br *J Pharmacol*. 2006;147(suppl 1):S232-240. https://doi.org/10.1038/sj.bjp.0706400

(11) Swanson RA, Ying W, Kauppinen TM. Astrocyte influences on ischemic neuronal death. *Curr Mol Med*. 2004;4:193-205. https://doi.org/10.2174/1566524043479185

(12) Wong CH1, Crack PJ. Modulation of neuro-inflammation and vascular response by oxidative stress following cerebral ischemia-reperfusion injury. *Curr Med Chem.* 2008;15:1-14. https://doi.org/10.2174/092986708783330665

(13) Faraco G, Fossati S, Bianchi ME, et al. High mobility group box 1 protein is released by neural cells upon different stresses and worsens ischemic neurodegeneration in vitro and in vivo. *J Neurochem*. 2007;103:590-603. https://doi.org/10.1111/j.1471-4159.2007.04788.x

(14) Arumugam TV, Okun E, Woodruff TM. Toll-like Receptors in Ischemia-Reperfusion Injury. *Shock*. 2009;32:4-16. https://doi.org/10.1097/SHK.0b013e318193e333

(15) Goering J, Pope MR, Sherry D Fleming. TLR2 Regulates Complement-Mediated Inflammation Induced by Blood Loss During Hemorrhage. *Shock.* 2016;45:33-39. https://doi.org/10.1097/SHK.0000000000000477

(16) Tang SC, Arumugam TV, Xu X, et al. Pivotal role for neuronal Toll-like receptors in ischemic brain injury and functional deficits. *Proc Natl Acad Sci USA*. 2007;104:13798-13803. https://doi.org/10.1073/pnas.0702553104

(17) Hua F, Ma J, Ha T, et al. Preconditioning with a TLR2 specific ligand increases resistance to cerebral ischemia/reperfusion injury. *J Neuroimmunol*. 2008;199:75-82. https://doi.org/10.1016/j.jneuroim.2008.05.009

(18) Winters L, Winters T, Gorup D, et al. (2013) Expression analysis of genes involved in TLR2-related signaling pathway: Inflammation and apoptosis after ischemic brain injury. *Neurosci*. 2013;238:87-96. https://doi.org/10.1016/j.neuroscience.2013.02.001

(19) Mottahedin A, Svedin P, Nair S, et al. Systemic activation of Toll-like receptor 2 suppresses mitochondrial respiration and exacerbates hypoxic-ischemic injury in the developing brain. *J Cereb Blood Flow Metab*. 2017;37:1192-1198. https://doi.org/10.1177/0271678X17691292

(20) Bergt S, Güter A, Grub A, et al. Impact of Toll-Like Receptor 2 deficiency on survival and neurological function after cardiac arrest: a murine model of cardiopulmonary resuscitation. PLoS One. 2013;8:e74944. https://doi.org/10.1371/journal.pone.0074944.eCollection 2013

(21) Dienel GA. Brain Glucose Metabolism: Integration of Energetics with Function. *Physiol Rev.* 2019;99:949-1045. https://doi.org/10.1152/physrev.00062.2017

(22) Mergenthaler P, Lindauer U, Dienel GA, Meisel A. Sugar for the brain: the role of glucose in physiological and pathological brain function. *Trends Neurosci.* 2013;36:587-97. https://doi.org/10.1016/j.tins.2013.07.001

(23) Wunder A, Klohs J, Dirnagl U. Non-invasive visualization of CNS inflammation with nuclear and optical imaging. *Neuroscience*. 2009;158(3):1161-1173. https://doi.org/10.1016/j.neuroscience. 2008.10.005

(24) Radu CG, Shu CJ, Shelly SM, Phelps ME, Witte ON. Positron emission tomography with computed tomography imaging of neuroinflammation in experimental autoimmune encephalomyelitis. *Proc Natl Acad Sci USA*. 2007;104:1937-1942. https://doi.org/10.1073/pnas.0610544104

(25) Szöllősi D, Hegedűs N, Veres DS, et al. Evaluation of Brain Nuclear Medicine Imaging Tracers in a Murine Model of Sepsis-Associated Encephalopathy. *Mol Imaging Biol*. 2018;20:952-962. https://doi.org/10.1007/s11307-018-1201-3

(26) Putzu A, Valtorta S, Di Grigoli G, et al. Regional Differences in Cerebral Glucose Metabolism After Cardiac Arrest and Resuscitation in Rats Using [18F]FDG Positron Emission Tomography and Autoradiography. *Neurocrit Care*. 2018;28:370-378. https://doi.org/10.1007/s12028-017-0445-0

(27) Zhang HJ, Mitchell S, Fang YH, et al. Assessment of Brain Glucose Metabolism Following Cardiac Arrest by [18F]FDG Positron Emission Tomography. *Neurocrit Care*. 2020 May 1;10. [epub ahead of print]. https://doi.org/10.1007/s12028-020-00984-6.

(28) Bergt S, Grub A, Müller M, et al. Toll-like receptor 4 deficiency or inhibition does not modulate survival and neurofunctional outcome in a murine model of cardiac arrest and resuscitation. *PLoS One*. 2019;14:e0220404. https://doi.org/10.1371/journal.pone.0220404.eCollection 2019

(29) Ma Y, Hof PR, Grant SC, et al. A three-dimensional digital atlas database of the adult C57BL/6J mouse brain by magnetic resonance microscopy. *Neuroscience*. 2005;135:1203-1215. https://doi.org/10.1016/j.neuroscience.2005.07.014

(30) Mirrione MM, Schiffer WK, Fowler JS, Alexoff DL, Dewey SL, Tsirka SE. A novel approach for imaging brain-behavior relationships in mice reveals unexpected metabolic patterns during seizures in the absence of tissue plasminogen activator. *Neuroimage*. 2007;38:34-42. https://doi.org/10.1016/j.neuroimage.2007.06.032

(31) de Lange C, Malinen E, Qu H, et al. Dynamic FDG PET for assessing early effects of cerebral hypoxia and resuscitation in new-born pigs. *Eur J Nucl Med Mol Imaging*. 2012;39:792-799. DOI: 10.1007/s00259-011-2055-y

(32) Li YQ, Liao XX, Lu JH, et al. Assessing the early changes of cerebral glucose metabolism via dynamic (18)FDG-PET/CT during cardiac arrest. *Metab Brain Dis*. 2015;30:969-977. https://doi.org/10.1007/s11011-015-9658-0

(33) Hoxworth JM, Xu K, Zhou Y, Lust WD, LaManna JC. Cerebral Metabolic Profile, Selective Neuron Loss, and Survival of Acute and Chronic Hyperglycemic Rats

Following Cardiac Arrest and Resuscitation. *Brain Res.* 1999;821:467-479. https://doi.org/10.1016/s0006-8993(98)01332-8

(34) Wu C, Li F, Niu G, Chen X. PET Imaging of Inflammation Biomarkers. *Theranostics*. 2013;3:448-466. Print 2013. https://doi.org/10.7150/thno.6592

(35) Lee WW, Marinelli B, van der Laan AM, et al. PET/MRI of Inflammation in Myocardial Infarction. *J Am Coll Cardiol.* 2012;59:153-163. https://doi.org/10.1016/j.jacc.2011.08.066

(36) Backes H, Walberer M, Ladwig A, et al. Glucose Consumption of Inflammatory Cells Masks Metabolic Deficits in the Brain. *Neuroimage*. 2016;128:54-62. https://doi.org/10.1016/j.neuroimage.2015.12.044

(37) Pektor S, Bausbacher N, Otto G, et al. Toll like receptor mediated immune stimulation can be visualized in vivo by [^{18}F]FDG-PET. *Nucl Med Biol.* 2016;43:651-660. https://doi.org/10.1016/j.nucmedbio. 2016.07.004

(38) Hosmann A, Schober A, Gruber A, et al. Cerebral and Peripheral Metabolism to Predict Successful Reperfusion After Cardiac Arrest in Rats: A Microdialysis Study. *Neurocrit Care.* 2016;24:283-93. https://doi.org/10.1007/s12028-015-0214-x

(39) Lu C, Liu L, Chen Y, et al. TLR2 Ligand Induces Protection against Cerebral Ischemia/Reperfusion Injury via Activation of Phosphoinositide 3-Kinase/Akt Signaling. J Immunol. 2011;187:1458-1466. https://doi.org/10.4049/jimmunol.1003428.

(40) Lehnardt S, Lehmann S, Kaul D et al. Toll-like receptor 2 mediates CNS injury in focal cerebral ischemia. J Neuroimmunol. 2007;190:28-33. https://doi.org/10.1016/j.jneuroim.2007.07.023

(41) Iram N, Mildner M, Prior M, et al. Age-related changes in expression and function of Toll-like receptors in human skin. Development. 2012;139:4210-4219. https://doi.org/10.1242/dev.083477

(42) Yoshizawa H, Gazes Y, Stern Y et al. Characterizing the normative profile of 18F-FDG PET brain imaging: sex difference, aging effect, and cognitive reserve. Psychiatry Res. 2014;221:78-85. https://doi.org/10.1016/j.pscychresns.2013.10.009

(43) Newberg AB, Alavi A. Normal Patterns and Variants in PET Brain Imaging. PET Clin. 2010;5:1-13. https://doi.org/10.1016/j.cpet.2009.12.006

(44) Bascuñana P, Thackeray JT, Bankstahl M, Bengel FM, Bankstahl JP. Anesthesia and Preconditioning Induced Changes in Mouse Brain [^{18}F] FDG Uptake and Kinetics. *Mol Imaging Biol.* 2019; 21:1089-1096. https://doi.org/10.1007/s11307-019-01314-9

(45) Abdel el Motal SM, Sharp GW. Inhibition of Glucose-Induced Insulin Release by Xylazine. *Endocrinology.*1985;116:2337-2340. https://doi.org/10.1210/endo-116-6-2337

(46) Jalloh I, Carpenter KLH, Helmy A, Carpenter TA, Menon DK, Hutchinson PJ. Glucose Metabolism Following Human Traumatic Brain Injury: Methods of Assessment and Pathophysiological Findings. *Metab Brain Dis.* 2015;30:615-632. https://doi.org/10.1007/s11011-014-9628-y

(47) Herholz K, Heiss WD. Positron emission tomography in clinical neurology. *Mol Imaging Biol.* 2004;6:239-69. https://doi.org/10.1016/j.mibio.2004.05.002

(48) Johnson NR, Condello C, Guan S, et al. Evidence for Sortilin Modulating Regional Accumulation of Human Tau Prions in Transgenic Mice. *Proc Natl Acad Sci USA*. 2017;114:E11029-E11036. https://doi.org/10.1073/pnas.1717193114

TABLES

Tab.1: Hemodynamic and physical parameters before and after CA-CPR and injected amount of tracer [^{18}F]FDG. Data shown as mean ± SEM. No significant difference was seen between experimental groups (Mann-Whitney *U* test) or between basal measurements and after CA-CPR (Wilcoxon rank-sum test). Injected quantity of [^{18}F]FDG tracer was almost the same for both groups and time points (WT, basal vs. after CA-CPR PET scan: p=0.878; WT vs. TLR2, basal PET scan: p=0.481; WT vs. TLR2, PET scan after CA-CPR: p=0.398).

FIGURE LEGENDS

Fig.1: Study protocol and timeline of experimental procedure. *[^{18}F]FDG - [^{18}F]fluordeoxyglucose, CA – cardiac arrest, CPR – cardiopulmonary resuscitation, CVC – central venous catheter, d – days, min – minutes, PET – positron emission tomography, TLR – toll-like receptor, TVC – tail venous catheter, WT – Wild Type.*

Fig.2: Representative examples of [^{18}F]FDG uptake images taken between 50 and 60 min after injection of tracer in WT- and TLR2$^{-/-}$-mouse brains basal and after CA-CPR.

Fig.3: Total cerebral uptake of [^{18}F]FDG measured in PET-CT for 1 hour. Absolute [^{18}F]FDG uptake (SUV) in WT- and TLR2$^{-/-}$ mouse brains were measured at baseline and after CA-CPR. Data shown as boxplots. * p value = 0.017 (Wilcoxon rank-sum test), # p value = 0.001 (Mann-Whitney U test).

Fig.4: Global cerebral metabolism measured using [^{18}F]FDG-PET-CT. Absolute [^{18}F]FDG uptake (SUV_{mean}) in WT- and TLR2$^{-/-}$ mouse brains was measured at baseline and after CA-CPR. Data shown as boxplots. * p value = 0.017 (Wilcoxon rank-sum test), # p value = 0.001 (Mann-Whitney U test).

Fig.5: Basal regional [^{18}F]FDG uptake in WT and TLR2$^{-/-}$ mice in absolute SUV. The absolute [^{18}F] FDG uptake values of basal PET scans in WT(white)- and TLR2$^{-/-}$ (black) mouse brain regions displayed in comparison. Data shown as SUV_{mean} ± SEM; p values were calculated using Mann-Whitney-U-test and Bonferroni correction. Absolute uptake [^{18}F]FDG uptake values WT vs. TLR2$^{-/-}$ mice (P-values): ^{*1} 0.000, ^{*2} 0.001, ^{*3} 0.002, ^{*4} 0.003, ^{*5} 0.005, ^{*6} 0.001, ^{*7} 0.001, ^{*8} 0.002, ^{*9} 0.009, ^{*10} 0.011, ^{*11} 0.002, ^{*12} 0.007, ^{*13} 0.000, ^{*14} 0.004.

Fig.6: Absolute regional cerebral metabolism measured using [^{18}F]FDG-PET-CT. a and c: Absolute [^{18}F]FDG uptake (SUV) in WT(**a**)- and TLR2$^{-/-}$(**c**) mouse brains were measured at baseline and after CA-CPR. Data shown as SUV_{mean} ± SEM. p values (Wilcoxon rank-sum test, Bonferroni corrected for WT (**a**): ^{*1} 0.017, ^{*2} 0.017, ^{*3} 0.017, ^{*4} 0.007, ^{*5} 0.017, ^{*6} 0.022, ^{*7} 0.013, ^{*8} 0.013. Because of Bonferroni correction hippocampus (p=0.037), central gray (p=0.028) and thalamus (p=0.028) failed significance in WT animals. p values (Wilcoxon rank-sum test, Bonferroni corrected for TLR2$^{-/-}$ mice (**c**):^{*a} 0.011, ^{*b} 0.011, ^{*c} 0.011, ^{*d} 0.021. Because of Bonferroni correction superior colliculi (p=0.038) failed significance in TLR2$^{-/-}$ mice. **b and d:** Percentage variation of absolute [^{18}F]FDG uptake in basal and CA-CPR measurements in WT (**b**) and TLR2$^{-/-}$(**d**) mice. **Inset:** Schematic representation of mouse brain regions subdivided in forebrain (red) and hindbrain (see 48): Ofl - olfactory bulb, Ctx - cortex, Str – striatum, Hip – hippocampus, Thl - Thalamus, Hyp - hypothalamus, Mdb - midbrain, Cbr - cerebellum, Bst - brain st

Tab.1

Parameter	experimental groups				p-values
	WT mice (n = 10)		**TLR2$^{-/-}$ mice** (n = 10)		
before CA-CPR	**basal**	**1.5 h after CA-CPR**	**basal**	**1.5 h after CA-CPR**	
heart rate [1/min]		222 ± 4		214 ± 9	0.136
MAP [mm Hg]		71.67 ± 4.79		80.75 ± 6.69	0.308
body temperature [°C]		35.89 ± 0.06		35.94 ± 0.05	0.932
CA-CPR					
ROSC time [s]		66.5 ± 8.6		72.5 ± 8.17	0.356
ROSC rate		100%		100%	
epinephrine [µg]		12.5 ± 1.12		13.5 ± 1.5	0.46
1 h after CA-CPR					
heart rate [1/min]		374 ± 33		311 ± 20	0.452
MAP [mm Hg]		48.33 ± 1.67		58.33 ± 6,01	0.518
body temperature [°C]		36.28 ± 0.08		36.22 ± 0.10	0.564
Mean [^{18}F]FDG [MBq]	16.65 ± 0.27	16.77 ± 0.67	17.44 ± 0.65	15.78 ± 0.51	heading
Range [MBq]	15.14 - 17.97	13.72 - 20.36	15.02 - 22.01	13.99 - 18.65	

Figures

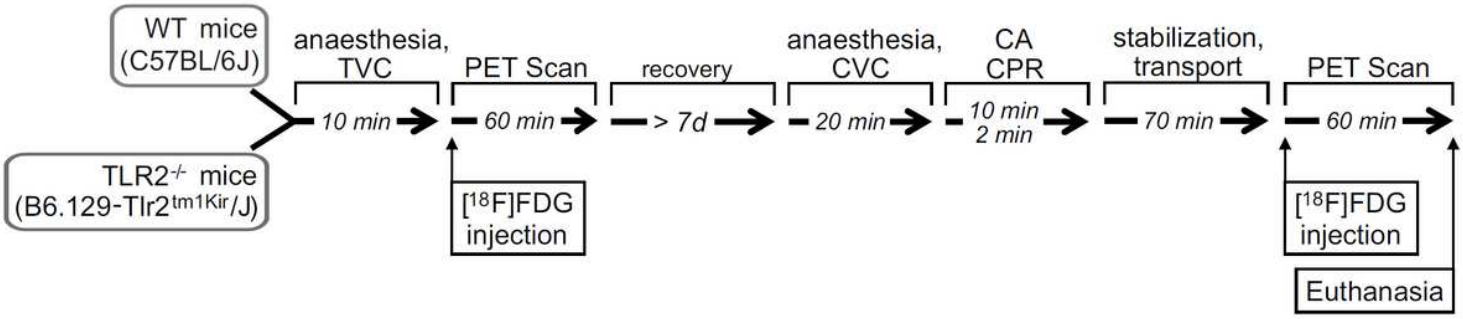

Figure 1

Study protocol and timeline of experimental procedure. [18F]FDG - [18F]fluordeoxyglucose, CA – cardiac arrest, CPR – cardiopulmonary resuscitation, CVC – central venous catheter, d – days, min – minutes, PET – positron emission tomography, TLR – toll-like receptor, TVC – tail venous catheter, WT – Wild Type.

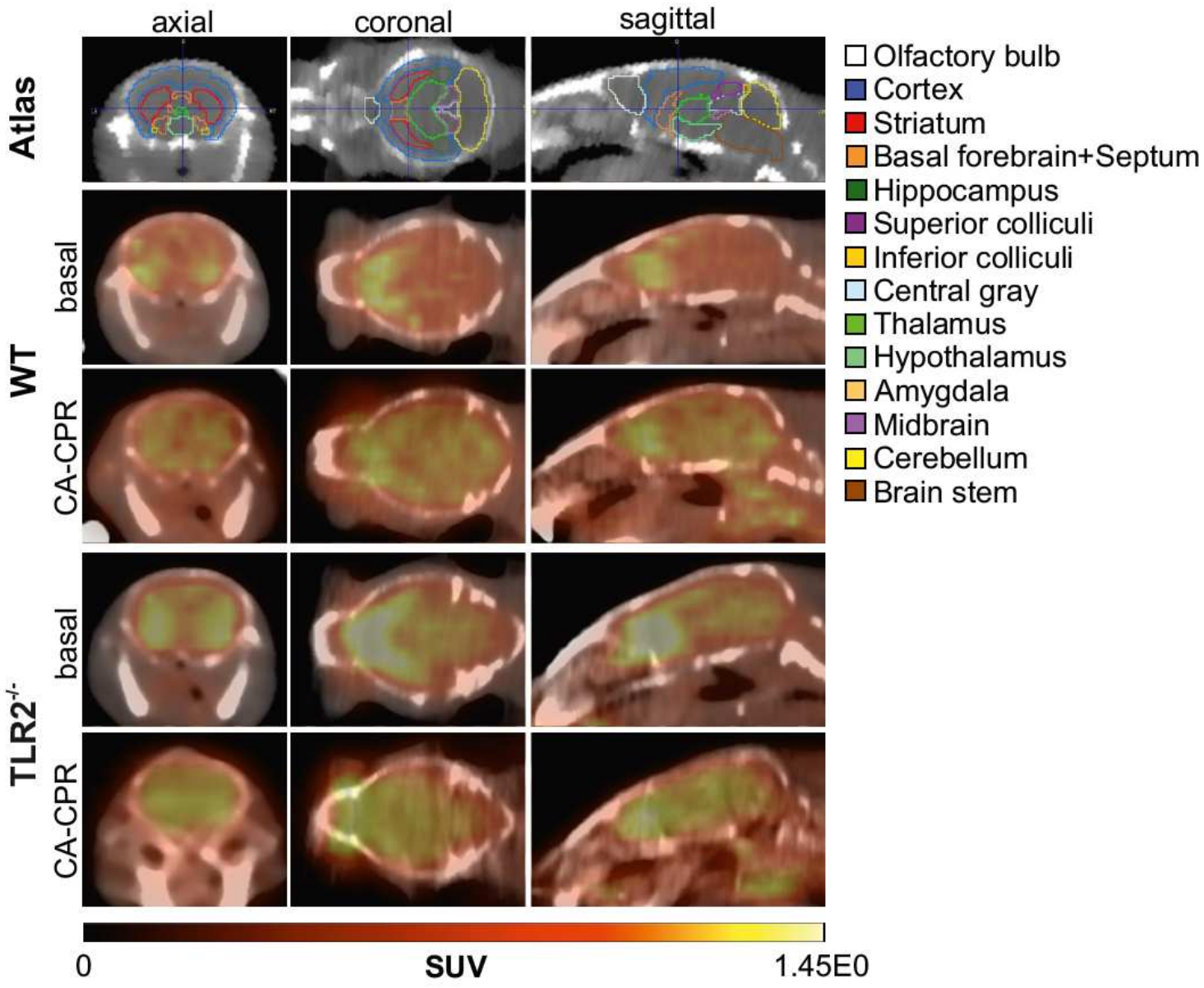

Figure 2

Representative examples of [18F]FDG uptake images taken between 50 and 60 min after injection of tracer in WT- and TLR2-/–mouse brains basal and after CA-CPR.

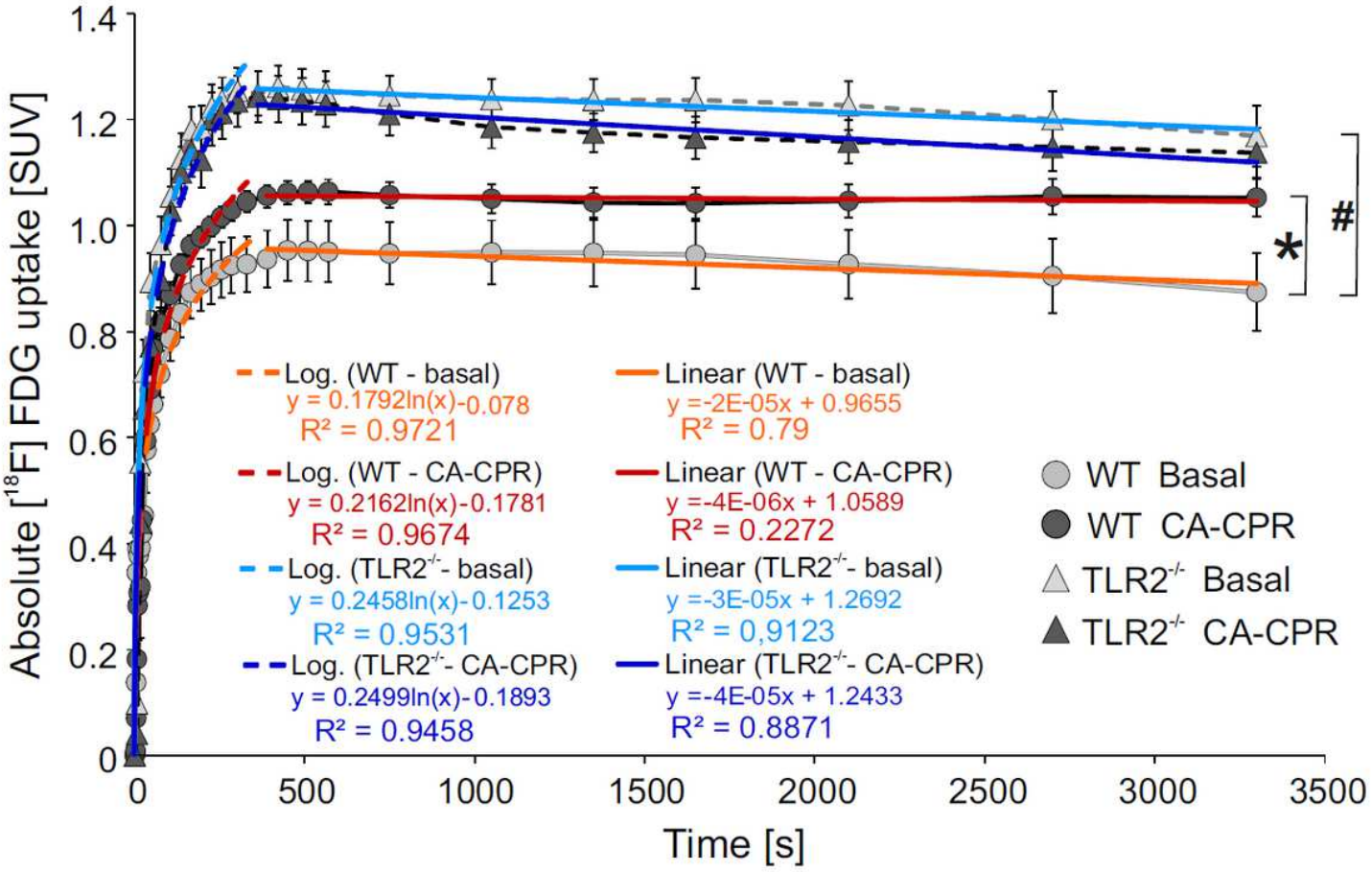

Figure 3

Total cerebral uptake of [18F]FDG measured in PET-CT for 1 hour. Absolute [18F]FDG uptake (SUV) in WT- and TLR2-/- mouse brains were measured at baseline and after CA-CPR. Data shown as boxplots. * p value = 0.017 (Wilcoxon rank-sum test), # p value = 0.001 (Mann-Whitney U test).

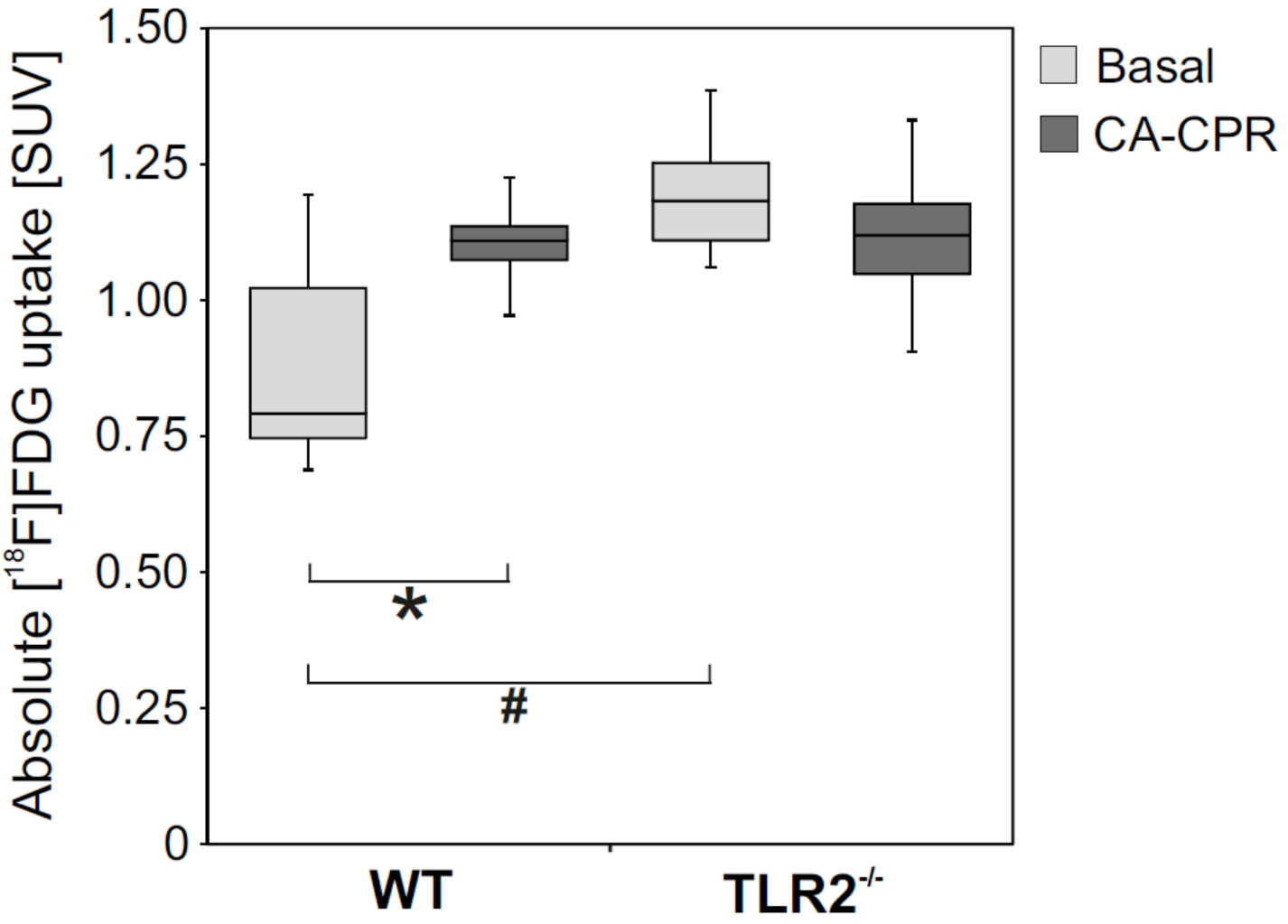

Figure 4

Global cerebral metabolism measured using [18F]FDG-PET-CT. Absolute [18F]FDG uptake (SUVmean) in WT- and TLR2-/- mouse brains was measured at baseline and after CA-CPR. Data shown as boxplots. * p value = 0.017 (Wilcoxon rank-sum test), # p value = 0.001 (Mann-Whitney U test).

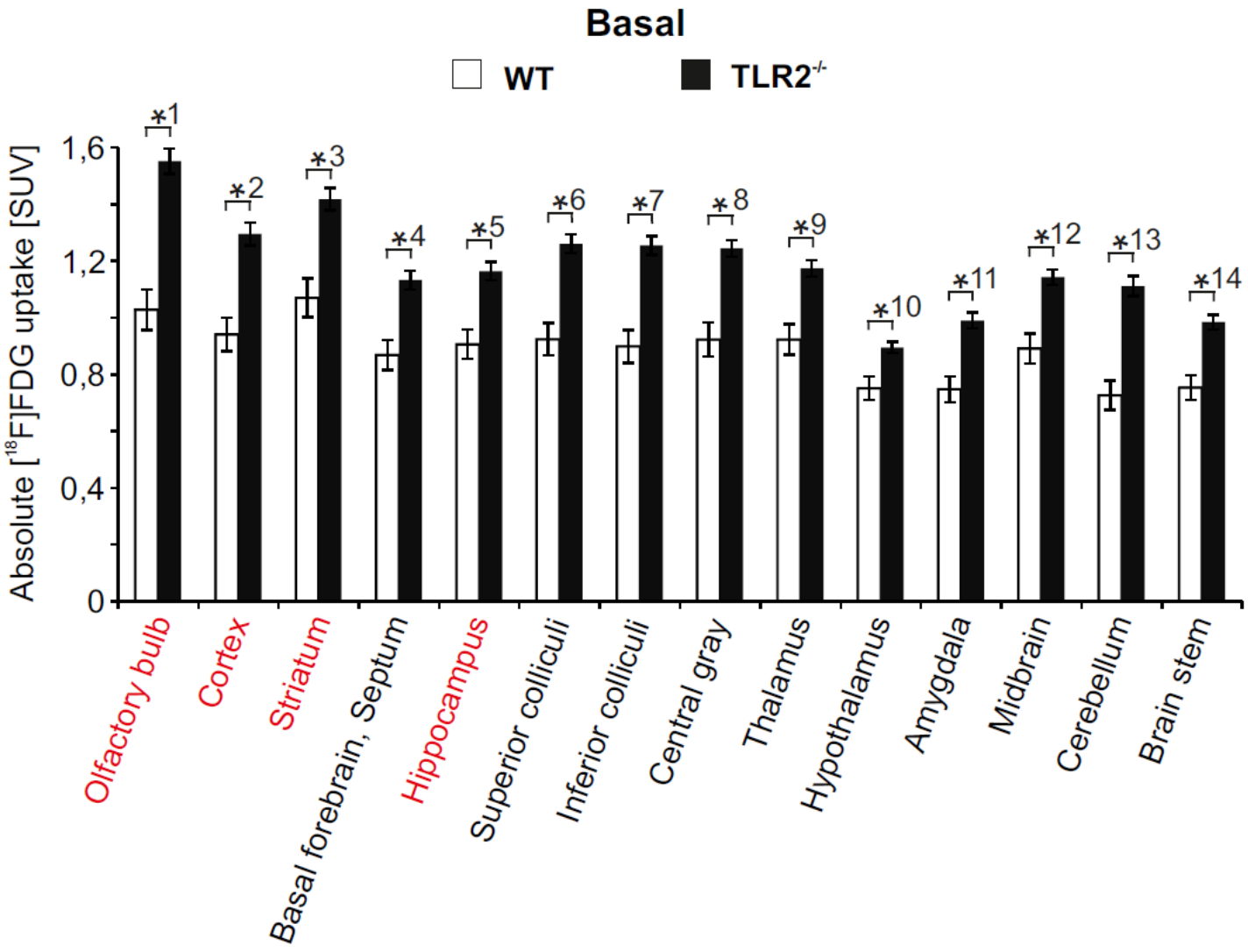

Figure 5

Basal regional [18F]FDG uptake in WT and TLR2-/- mice in absolute SUV. The absolute [18F] FDG uptake values of basal PET scans in WT(white)- and TLR2-/- (black) mouse brain regions displayed in comparison. Data shown as SUVmean ± SEM; p values were calculated using Mann-Whitney-U-test and Bonferroni correction. Absolute uptake [18F]FDG uptake values WT vs. TLR2-/- mice (P-values): *1 0.000, *2 0.001, *3 0.002, *4 0.003, *5 0.005, *6 0.001, *7 0.001, *8 0.002, *9 0.009, *10 0.011, *11 0.002, *12 0.007, *13 0.000, *14 0.004.

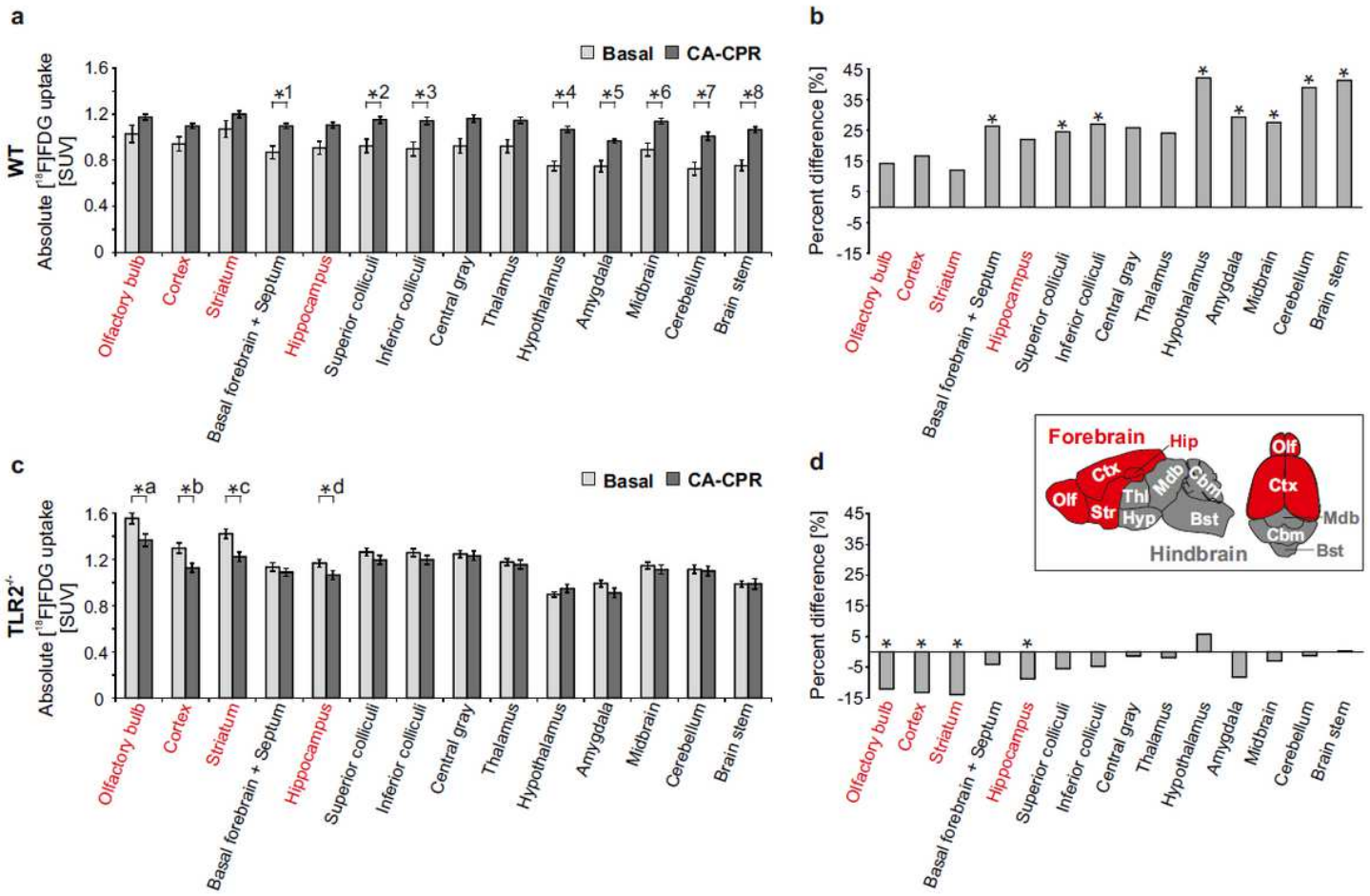

Figure 6

Absolute regional cerebral metabolism measured using [18F]FDG-PET-CT. a and c: Absolute [18F]FDG uptake (SUV) in WT(a)- and TLR2-/-(c) mouse brains were measured at baseline and after CA-CPR. Data shown as SUVmean ± SEM. p values (Wilcoxon rank-sum test, Bonferroni corrected for WT (a): *1 0.017, *2 0.017, *3 0.017, *4 0.007, *5 0.017, *6 0.022, *7 0.013, *8 0.013. Because of Bonferroni correction hippocampus (p=0.037), central gray (p=0.028) and thalamus (p=0.028) failed significance in WT animals. p values (Wilcoxon rank-sum test, Bonferroni corrected for TLR2-/- mice (c):*a 0.011, *b 0.011, *c 0.011, *d 0.021. Because of Bonferroni correction superior colliculi (p=0.038) failed significance in TLR2-/- mice. b and d: Percentage variation of absolute [18F]FDG uptake in basal and CA-CPR measurements in WT (b) and TLR2-/-(d) mice. Inset: Schematic representation of mouse brain regions subdivided in forebrain (red) and hindbrain (see 48): Ofl - olfactory bulb, Ctx - cortex, Str – striatum, Hip – hippocampus, Thl - Thalamus, Hyp - hypothalamus, Mdb - midbrain, Cbr - cerebellum, Bst - brain st